ADVANCED MATERIALS
www.advmat.de

Materials Views
www.MaterialsViews.com

Photoinduced Memory with Hybrid Integration of an Organic Fullerene Derivative and an Inorganic Nanogap-Embedded Field-Effect Transistor for Low-Voltage Operation

*Chung-Jin Kim, Sung-Jin Choi, Sungho Kim, Jin-Woo Han, Hoyeon Kim, Seunghyup Yoo, and Yang-Kyu Choi**

Conventional flash memory faces serious technical challenges in reducing high program/erase voltages,[1] and the increasing discrepancy between low supply voltages and the high flash-operation voltage makes problems worsen. They arise from the inherent trade-off relationship between the program/erase speed and retention time through the scaling of a tunnel oxide.[2] Moreover, it is forecasted that the reduction of the operation voltage will barely be achieved, despite aggressive dimensional scaling of the cell size.[3]

Recently, as an alternative memory mechanism, optical switching devices with a photoactive material have been proposed.[4–6] However, these optoelectronic approaches based on the simple functionalization or the homogeneous integration of organic channel/organic-based gate dielectrics still show intrinsic problems in memory functionality, such as unstable hysteresis, which make the data states undistinguishable and the operation voltage too high.

To be free from the aforementioned inherent limitations for low-voltage operation and the intrinsic problems stemming from the homogeneous integration of the organic material alone, it is essential to develop a novel operation method and hybrid integration based on the adoption of a new material such as a photoactive organic on a commercially matured and reliable silicon-based complementary metal oxide semiconductor (CMOS). On the other hand, although commercialized silicon-based CMOS devices provide high mobility and high-quality gate dielectrics accompanied with matured mass-production technology, hybrid integration is hampered by the high-temperature processes of CMOS, which can result in the thermal instability of organic materials.

Herein, we demonstrate a photoinduced memory for low-voltage operation, achieved by embedding an organic fullerene derivative, [6,6]-phenyl-C_{61}-butyric acid methyl ester (PCBM), into an inorganic nanogap. The nanogap structure paves the way for a high mobility corresponding with that of a silicon channel and organic-inorganic-hybrid integration without any thermal-instability issues in the organic material. Furthermore, the operation voltage, in the photoelectrical program/erase method, is noticeably reduced compared with that by the electrical program/erase method alone.[3] This is achieved by optically induced carrier injection with the aid of the photosensitive PCBM and retained free carriers, which are confined by PCBM-surrounding high-quality SiO_2. In view of the bias polarity and performance, the proposed program/erase mechanism, which is totally different from the mechanism relying on the electrical program/erase method only, is also verified using a commercialized numerical simulator.[7]

For optical carrier injection, PCBM is used as a photoreceptor in the proposed nanogap-embedded hybrid memory device. PCBM is a good candidate for optoelectronic applications due to its high extinction coefficient, which exceeds 10^4–10^5 cm^{-1}.[8] The implementation of organic materials that are vulnerable to high temperature in the inorganic CMOS process, however, should be avoided, or the process should be carefully designed so as to minimize thermally induced performance degradation, as well as possible cross contamination. A nanogap made by partial removal of a sacrificial gate dielectric can be one solution, because the nanogap can be filled following the high-temperature CMOS processes. Moreover, the formation of a nanogap filled with PCBM requires only three extra process steps: wet-etching to carve the nanogaps, thermal reoxidation, and the introduction of PCBM into the nanogaps by dipping or drop-casting (**Figure 1**a). Also, it should be noted that the nanogap structure exhibits a high mobility property, which cannot be acquired in conventional organic FETs (OFETs), and results from the organic-embedded-nanogap configuration based on a high-mobility inorganic (i.e., single crystalline) silicon template (see inset of **Figure 2**a and Supporting Information, Figure S1).

In the nanogap-filling process, the solution processability of PCBM is critical, because it enables the filling of the nanogaps with organic material by capillary force, as described in previous work.[9] As shown in the magnified transmission electron microscopy (TEM) image (inset of Figure 1b) the oxide-surrounded nanogap was well filled with PCBM without any voids, which resulted from the aforementioned high solubility[10] and small molecular dimensions of the PCBM, comparable to that of fullerene, C_{60}.[11] The nanogap length released by a buffered oxide etchant (BOE) was 500 nm, and the dimensions of the gate stack were 3.5 nm/35 nm/5.5 nm for the bottom (or tunneling) oxide/PCBM/top (or control) oxide, respectively (Figure 1b). Cross-sectional energy dispersive X-ray spectroscopy (EDS) mapping (Supporting Information, Figure S2a) confirmed that the nanogap-embedded material, sandwiched between the two oxide layers, contained carbon elements. Also, the Raman spectrum was recorded for PCBM

C.-J. Kim, S.-J. Choi, S. Kim, Dr. J.-W. Han, H. Kim, Prof. S. Yoo, Prof. Y.-K. Choi
Department of Electrical Engineering
KAIST, 335 Gwahangno, Yuseong-gu, Daejeon 305-701, Korea
E-mail: ykchoi@ee.kaist.ac.kr

DOI: 10.1002/adma.201101034

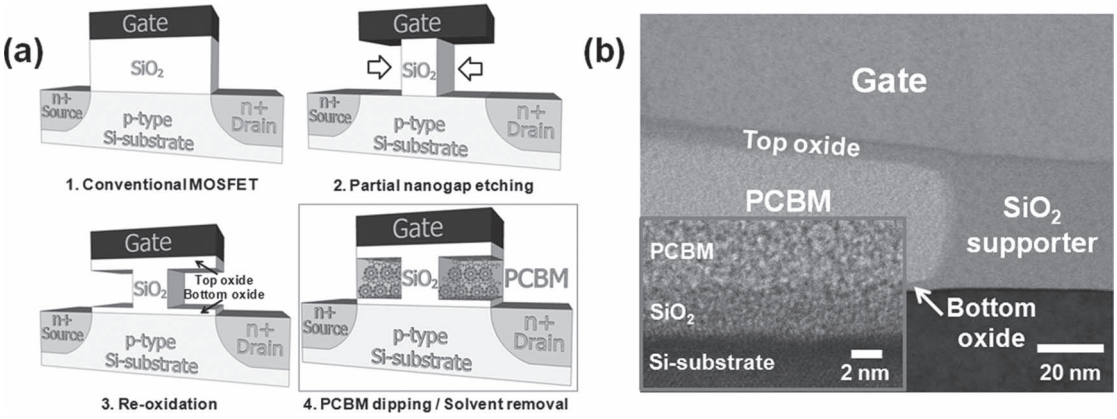

Figure 1. a) Schematic illustration depicting the fabrication process: PCBM-embedded photoinduced memory from conventional metal oxide semiconductor FET (MOSFET). b) Cross-sectional TEM image with 35 nm-thick PCBM. The inset shows the magnified TEM image at the bottom oxide interface.

(Supporting Information, Figure S2b) and the peak distribution at 1465 cm^{-1} (i.e., the ν (C=C) band) supported that the detected substance was PCBM.[12]

As a result of the optical-carrier injection in PCBM, the optical response of the proposed device appeared as a change in its threshold voltage (V_T), as shown in Figure 2a. For memory

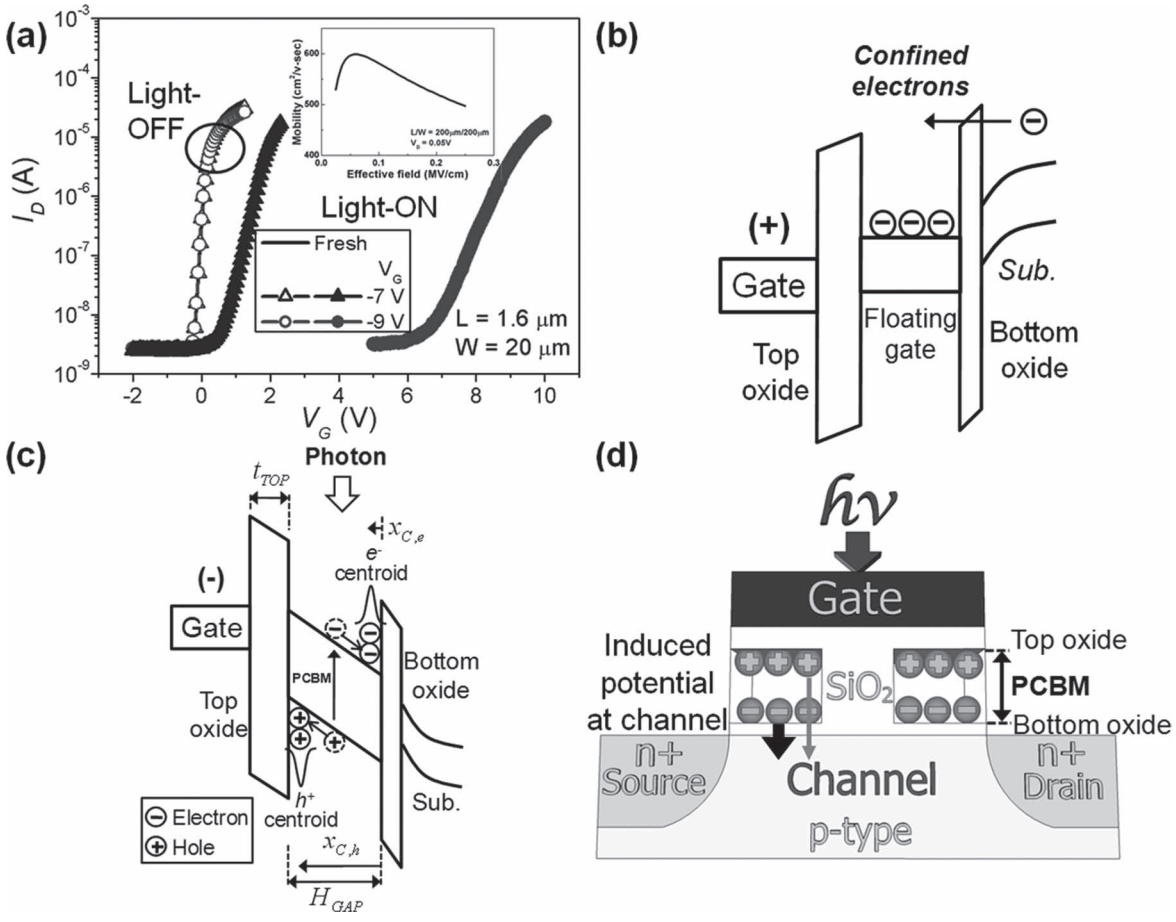

Figure 2. a) Measured transfer characteristics after gate-bias application of –7 V and –9 V with/without an optical pulse of 100 mW cm^{-2} by a halogen lamp (measurement sequence: 1. gate-voltage sweep; 2. negative gate voltage + optical pulse; and 3. gate-voltage sweep) b) Electrical-program method alone. c) Energy-band diagram that schematizes the behavior of e^- and h^+ during application of the (–) gate bias using the photoelectrical-program method. d) Schematic to illustrate the operation principle of the photoinduced memory. The different distances of e^- and h^+ from the channel result in a spatially imbalanced charge effect.

functioning, the V_T of the proposed device was uniquely shifted by the application of a relatively low negative bias with the aid of an optical stimulus, whereas it was shifted by the application of a high positive bias in a conventional n-channel non-volatile memory (NVM) device.[13] When a high negative gate bias was applied alone, no change in the transfer characteristics was observed (empty symbols). If, however, the same negative-gate pulse of –9 V and an optical pulse (white light, 100 mW cm^{-2}, see Experimental Section) were applied together, referred to as the photoelectrical program, a V_T shift (ΔV_T) in excess of 9 V was observed and the amount of the shift was enhanced with increased negative-gate voltage (filled symbols).

When light is irradiated on photosensitive PCBM, similar to an organic photovoltaic (OPV) device,[14] excitons or electron-hole pairs bound by the Coulomb force are formed. Free electrons (e^-) and holes (h^+), which are separated by the applied electric field, then move towards the opposite ends of the PCBM layer and accumulate at the bottom oxide/PCBM and the top oxide/PCBM interfaces under a negative voltage, respectively, as shown in Figure 2c. As long as the same number of e^- and h^+ remain, they cannot contribute to the excess charges that induce a ΔV_T, as in conventional flash memory using Fowler–Nordheim tunneling (FNT): the conventional FNT-program method is based on tunneling through the triangular-shaped barrier by the electric field (Figure 2b). For that tunneling, a highly positive gate bias, enough to make a narrow barrier, is required; electrons, that are selectively tunneled into the electrically isolated floating gate from the inverted channel, make a positive shift of the threshold voltage. In contrast, the photoelectrical-program method firstly creates the electron-hole pairs through the light illumination and, secondly, separates them through the electric voltage. Those redistributed e^- and h^+ result in a V_T shift because of the differently induced potential at the channel, which arises from the accumulated e^- and h^+ at the interface. It should be noted that the induced potential by the charges at the bottom oxide/PCBM interface is not the same as that by the charges at the top oxide/PCBM interface because it is a function of the distance from the channel. Therefore e^- close to the channel have a greater influence on the channel potential than h^+ close to the gate do, as shown in Figure 2d. This spatially imbalanced charge distribution eventually contributes to a ΔV_T, even if the numbers of e^- and h^+ remain the same within the PCBM layer. The ΔV_T, induced by the separated charges, can be described by:[15]

$$\Delta V_T = -\frac{Q_e}{A\varepsilon_{OX}}(x_{C,h} - x_{C,e}) \quad (1)$$

In Equation 1, Q_e is the amount of electron charges, the value of which is the same as that of the hole charges and is proportional to the nanogap area occupied by the PCBM; A is the device area, which is expressed as the product of the gap length and the device width; ε_{ox} is the permittivity of SiO_2, and $x_{C,e}$ and $x_{C,h}$ are the centroids of the confined e^- and h^+, which are the respective distances from the channel interfaces (Supporting Information). Equation 1 is consistent with the proposed spatially imbalanced charge distribution and the charge-based numerical simulations (Supporting Information, Figure S3).

As explained in Figure 2c, the combination of both a negative electrical pulse and an optical pulse is required for a positive ΔV_T, which is the photoelectrical program. If we simply change the polarity of the gate pulse, namely the application of a positive electrical pulse with the optical pulse, V_T shifts oppositely and it can be named as a photoelectrical erase. The decreased V_T results from the decreased number of e^- in the company of h^+ by sequential processes of the generated excitons dissociation and recombination with e^- and h^+ that had been formerly distributed at the interface by the photoelectrical program (Supporting Information, Figure S4). In short, it can be concluded that the optical pulse acts as a driving force for ΔV_T and the electrical pulse acts as a controller to determine on/off switching, the direction of the shift, and the operation speed. This kind of controllable method, which uses electrical and optical pulses simultaneously for program/erase, can overcome the limitation of previous similar work using an optical or electrical pulse alone for program and erase;[16] thereby, it can be a strength over other work, as well as the compatibility with traditional Si-technology for mass production.

Figure 3a,b shows the program and erase speed of the photoinduced memory for various gate pulses. The switching speed means the time duration over which the optical and the electrical pulses were applied simultaneously. As the magnitude of the gate pulse increased, the V_T difference increased. Notably, a low program/erase operation voltage, equivalent to 2 MV cm^{-1} of electric field, is the merit of the proposed memory. Compared with the conventional FNT method for NVM programming, the photoelectrical-program method resulted in a lowered operation voltage and a bigger ΔV_T (Supporting Information, Figure S5). A greater shift of the threshold voltage with a lowered program voltage is highly demanded to sustain an exponential growth rate in the memory market for the next two decades.

The data retainability could be examined by observing the evolution of V as a function of time, as shown in Figure 3c. In the absence of an external pulse after the photoelectrical-program process, the duration of the memory effect could be estimated, given that the imbalanced charge distribution was retained. If we extrapolate the transition curve of V_T to 10 years, which is the retention criterion for commercial flash memory, it is observed that 50% of the photoinduced charges, expressed as the V_T difference, are preserved. Recombination through back transfer of e^- and h^+[17] and charge loss due to the low barrier height of the oxide seen by e^-, owing to the lowest-unoccupied-molecular-orbital (LUMO) level of the PCBM,[18,19] can be considered as two of the reasons for V_T relaxation. Figure 3 d shows the repeatability of the photoinduced memory in a single device and it was observed that data were well preserved after 1000 on/off cycles. The reason that V_T seemed to gradually increase is due to the degradation of the transfer curve (subthreshold swing), which was induced from interface trapping during the repeatable accumulation process of the photoinduced charges. The endurance property, including the voltage shift, will be improved through the optimization of generated excitons, such as light-intensity tuning and program/erase-voltage lowering.

Due to the photosensitive nature of the operation mechanism, the proposed device can also act as a photodetector. To verify the feasibility as a photodetector, the spectral photoresponse and the intensity dependence were characterized.

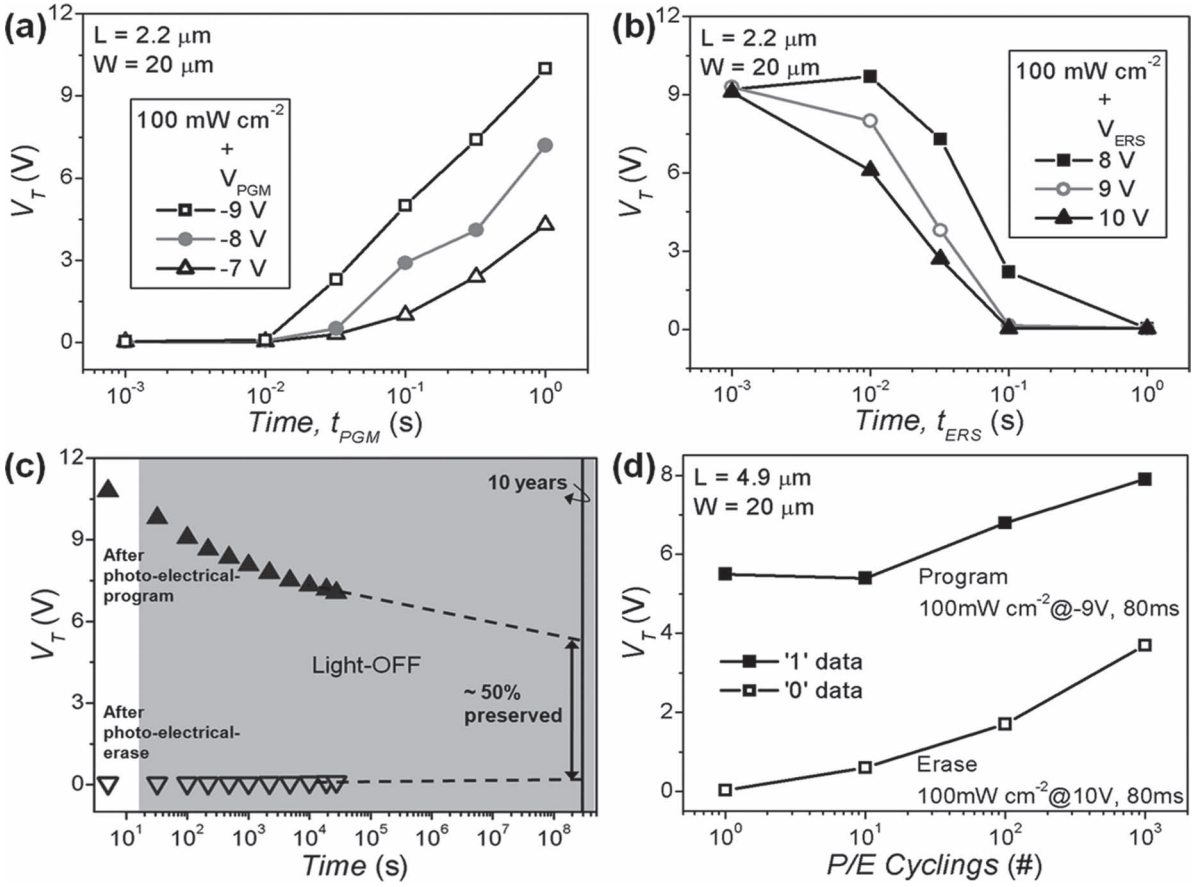

Figure 3. a) Program speeds for various gate voltages with fixed light intensity. b) Erase speeds for various gate voltages with a fixed light intensity. c) Data-retainability characteristics without electrical and optical pulses after photoelectrical programming and photoelectrical erase. d) Repeatability characteristics with respect to the number of program/erase operations.

Figure 4a shows the spectral dependence of the proposed photoinduced memory. A wavelength-dependent ΔV_T is clearly observed. Red-, green-, and blue-colored light-emitting diode (LED) (30 mW cm^{-2} each) light sources were used for this spectral study. As the wavelength of the incident light decreased, the photoinduced memory effect increased. This is consistent with the characteristic that the absorbance of PCBM is higher in the shorter wavelength region,[20] since the number of generated excitons is proportional to the absorbance.

In observing the intensity dependence, the gate voltage necessary for light detection was designated as V_{DET}. The gate-bias-dependent characteristics in Figure 4b show the limit of detection in the optical intensity. It was observed that the margin for optical detection, the V_T difference between V_T in the initial state and after photoelectrical programming, decreased as the optical intensity decreased. Additionally, the margin for detection of a relatively low intensity could be acquired at the cost of a high V_{DET}. In addition to this improved detection ability to sense low-intensity light, the proposed configuration of photoinduced memory is applicable as a highly scaled image sensor. One unit pixel in a conventional image sensor is composed of a light-receiving photodetector region occupying a large area, because a silicon-based photodetector needs enough light for light sensing, and thus the enlarged area of the photodetector limits the scaling of each pixel. If the proposed scheme with an embedded photodetector were used for an image sensor, the pixel size would no longer be a concern.

As the next step, we investigated the effect of embedded organic materials on memory phenomena. It is known that the high degree of symmetry in C_{60}, as shown in the chemical structures in the inset of Figure 4c, results in many of the low-energy transitions being forbidden.[21,22] In contrast, C_{70}-based PCBM ([70]PCBM), with an asymmetric chemical structure, has a considerably higher extinction coefficient than C_{60}-based PCBM ([60]PCBM), which is directly tied to photon absorption; this results in more absorption in the visible wavelength region (Figure 4c).[8,22,23] It should be noted that the absorption spectrum of the halogen lamp used for the experiment was distributed primarily in the visible-light range. This characteristic appeared as a difference in the memory effect, as shown in Figure 4d. The critical gate bias in the [70]PCBM-embedded device that starts to enable a photoinduced memory effect was –3 V, while that of the [60]PCBM-embedded device was –7 V.

In conclusion, we have reported on photoinduced memory effects even at lowered voltages, by the use of simple hybrid integration with a photosensitive PCBM and embedded,

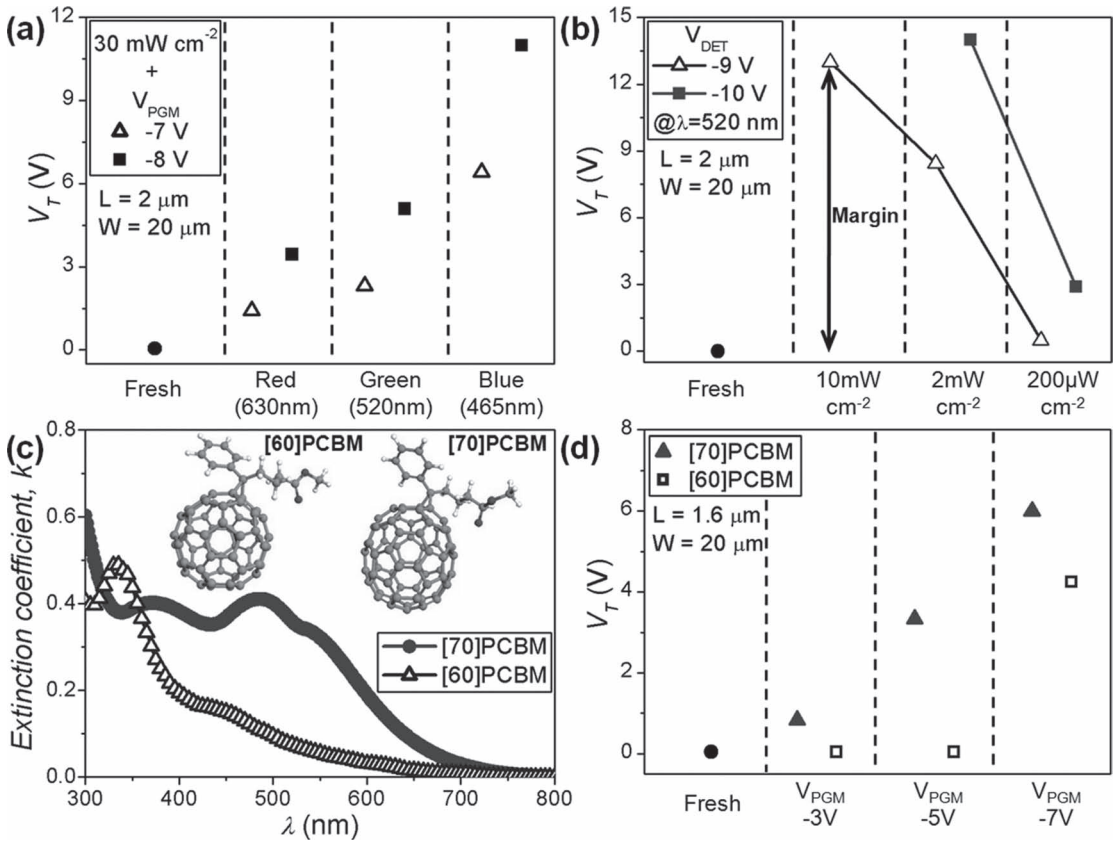

Figure 4. a) Wavelength dependence with red (630 nm), green (520 nm), and blue (465 nm) LED light sources. b) Intensity dependence of the photo-induced memory. c) Absorption spectra of [60]PCBM and [70]PCBM. The inset indicates the chemical structures of [60]PCBM and [70]PCBM. d) Memory effect according to the embedded material in the nanogap using a halogen lamp.

inorganic, silicon nanogaps. Based on experiments and simulations, we found that the photoinduced memory effect with a low operation voltage can be attributed to an imbalance in the spatial distribution of e^- and h^+ within the nanogap, where e^- and h^+ are separated from the photoinduced excitons. The proposed memory configuration will help guide research for high-performance memory applications and also provide a scaled scheme of a photodetector, based on the investigation of the spectral photoresponse and the ntensity dependence.

Experimental Section

For PCBM preparation, PCBM solution (5mg mL^{-1}, Nano-C) dissolved in chlorobenzene was stirred for 12 h, and filtered through a 0.2 μm polytetrafluoroethylene (PTFE) filter. The devices were dipped for 24 h and then dried at 150 °C for 1 h. The PCBM preparation and the coating process were performed under a nitrogen atmosphere inside a glove-box system.

The experiment for the optical response was performed using a halogen lamp, a light-emitting diode (LED), and a laser. The intensity of the halogen lamp (Hoya–Schott, Megalight 100), which was a broad-band light source, was measured using a fiber-optic spectrometer (K-MAC UV–vis Spectrometer, SV2100) and a calibrated photodiode (Thorlabs, FDS1010-CAL) of which the spectral response was known. Light from the halogen lamp was guided by an optical fiber and focused onto the sample using the objective lens of a microscope. For green light, a diode-pumped solid-state (DPSS) laser with a wavelength of 532 nm and a spectral line-width of 0.1 nm was used. Its intensity was varied using a neutral density (ND) filter. The intensity of the LED light source (Photron, 3 W Power LED) was modulated by the supplied voltage of the power supply (Agilent, E3646A) while monitoring the photocurrent of the calibrated photodiode. Since the viewing angle of an LED can be as large as 125°, an appropriate focusing lens was used to concentrate the light.

The electrical characteristics were analyzed using a parameter analyzer (Agilent, 4156C) and the drain current was measured while the gate voltage was swept with a grounded source voltage and a drain voltage of 0.1 V. To evaluate the memory performance, V_T was defined from the gate voltage corresponding to a constant drain current of 10^{-6} A μm^{-1}. A nominal electrical pulse was applied with medium integration time and stress mode was used for the characterization of the program and erase speed.

The TEM images were attained using a field-emission scanning TEM (Hitachi, HD-2300A). High-resolution TEM images were obtained at 200 kV and EDS elemental mapping was conducted (Supporting Information, Figure S1a).

Raman spectroscopy (NT-MDT, NTEGRA Spectra) was performed using a Renishaw Raman microscope with a 532 nm pumped solid-state laser and gratings of 600 lines mm^{-1}. The Raman spectra of the PCBM-coated samples were recorded by dipping a bulky silicon substrate into PCBM solution, which is the same as the dipping process of a photoinduced memory device.

Supporting Information

Supporting Information is available from the Wiley Online Library or from the author.

Acknowledgements

This work was partially supported by the IT R&D program of MKE/KEIT (10029953, Terabit Nonvolatile Memory Development) and a National Research Foundation of Korea (NRF) grant funded by the Korean Ministry of Education, Science and Technology (MEST) (No. 2009-0083079). The work was also supported by the Human Resource Training Project for Strategic Technology by the Korea Institute for Advancement of Technology (KIAT).

Received: March 21, 2011
Revised: April 27, 2011
Published online: June 10, 2011

[1] R. Bez, E. Camerlenghi, A. Modelli, A. Visconti, *Proc. IEEE* **2003**, *91*, 489.
[2] D. C. Gilmer, N. Goel, H. Park, C. Park, S. Verma, G. Bersuker, P. Lysaght, H.-H. Tseng, P. D. Kirsch, K. C. Saraswat, R. Jammy, *IEEE International Electron Devices Meeting*, Baltimore, USA, **2009**, 1.
[3] *Process Integration, Devices, and Structures*; International Technology Roadmap for Semiconductors, 2009; http://www.itrs.net/Links/2009ITRS/2009Chapters_2009Tables/2009Tables_FOCUS_C_ITRS.xls, accessed March 2011.
[4] A. Star, Y. Lu, K. Bradley, G. Gruner, *Nano Lett.* **2004**, *4*, 1587.
[5] C. B. Winkelmann, I. Ionica, X. Chevalier, G. Royal, C. Bucher, V. Bouchiat, *Nano Lett.* **2007**, *7*, 1454.
[6] S. Dutta, K. S. Narayan, *Adv. Mater.* **2004**, *16*, 2151.
[7] *Taurus Medici User Guide*, Synopsys Inc., Mountain View, CA, 2007.
[8] H. Hoppe, N. S. Sariciftci, D. Meissner, *Mol. Cryst. Liq. Cryst.* **2002**, *385*, 113.
[9] S.-W. Ryu, C.-J. Kim, M. Seo, C. Yun, S. Yoo, Y.-K. Choi, *Small* **2010**, *6*, 1617.
[10] C. Waldauf, P. Schilinsky, M. Perisutti, J. Hauch, C. J. Brabec, *Adv. Mater.* **2003**, *15*, 2084.
[11] H. W. Kroto, J. R. Heath, S. C. O'Brien, R. F. Curl, R. E. Smalley, *Nature* **2003**, *318*, 162.
[12] A. Dzwilewski, T. Wågberg, L. Edman, *J. Am. Chem. Soc.* **2009**, *131*, 4006.
[13] S. M. Sze, *Physics of Semiconductor Devices, Third edition*, Wiley, New York, **1981**, 227.
[14] C. J. Brabec, N. S. Sariciftci, J. C. Hummelen, *Adv. Funct. Mater.* **2001**, *11*, 15.
[15] A. Arreghini, F. Driussi, E. Vianello, D. Esseni, M. J. van Duuren, D. S. Golubovi , N. Akil, R. van Schaijk, *IEEE Trans. Electron Devices.* **2008**, *55*, 1211.
[16] J. Borghetti, V. Derycke, S. Lenfant, P. Chenevier, A. Filoramo, M. Goffman, D. Vuillaume, J.-P. Bourgoin, *Adv. Mater.* **2006**, *18*, 2535.
[17] S. S. Sun, *Sol. Energy Mater. Sol. Cells* **2005**, *85*, 261.
[18] Z. Liu, C. Lee, V. Narayanan, G. Pei, E. C. Kan, *IEEE Trans. Electron Devices* **2002**, *49*, 1606.
[19] O. Solomeshch, Y. J. Yu, A. A. Goryunkov, L. N. Sidorov, R. F. Tuktarov, D. H. Choi, J.-I. Jin, N. Tessler, *Adv. Mater.* **2009**, *21*, 4456.
[20] S. Cook, H. Ohkita, Y. Kim, J. J. Benson-Smith, D. D. C. Bradley, J. R. Durrant, *Chem. Phys. Lett.* **2007**, *445*, 276.
[21] M. A. Thompson, M. A. Argus, Lab 4.0, Planaria Software LLC, Seattle, WA, http://www.arguslab.com, **2004**.
[22] M. M. Wienk, J. M. Kroon, W. J. H. Verhees, J. Knol, J. C. Hummelen, P. A. van Hal, R. A. J. Janssen, *Angew. Chem. Int. Ed.* **2003**, *42*, 3371.
[23] S. Han, S. Lim, H. Kim, H. Cho, S. Yoo, *IEEE J. Selected Topics Quantum Electron.* **2010**, *16*, 1656.